Internal boundary layers in the ocean circulation

Lecture 10 by Jan Zika

This section follows on from Andy's 'Internal boundary layers in the ocean circulation'.

1 Equations of motion in the equatorial region

We may now define the scaled boundary layer equations

$$-(y+\zeta_n)v_n = -\frac{\partial B_n}{\partial y} \quad , \quad \zeta_n = -\frac{\partial u_n}{\partial y}. \tag{1}$$

Here the Bernoulli potential is defined as

$$B_n = P_n + \frac{1}{2}u_n^2 \tag{2}$$

and close to the equator we assume the relative vorticity is dominated by its local component $-\frac{\partial u}{\partial y}$. Beneath the surface, the streamfunction (ψ) may be defined on each layer such that

$$h_n \vec{u}_n = \hat{k} \times \nabla \psi_n. \tag{3}$$

We also define the potential vorticity

$$q_n = \frac{y - \frac{\partial u_n}{\partial y}}{h_n}, \tag{4}$$

which is the combination of both the planetary and relative components of vorticity. By combining (3) and (5), the streamfunction and Bernoulli function may be related by

$$q_n \frac{\partial \psi_n}{\partial x} = \frac{\partial B_n}{\partial x}, \tag{5}$$

and combined with zonal geostrophy ($yu_n = -\frac{\partial P_n}{\partial y}$) equation (4) may be extended to

$$q_n \nabla \psi_n = \nabla B_n. \tag{6}$$

Here the gradient of the Bernoulli function is related to the motion of potential vorticity. Although B_n is a closely related to streamfunction in rotating flows, in areas of no rotation this is not so (i.e. consider a non rotating flow where $q_n = 0$ hence B_n is a constant whereas there can by a complicated function for the flow (ψ) but for a rotating fluid the functions are intimately linked). By taking the dot product of $\vec{u}_n$ on both sides of (6), we may derive the following relationships in the equatorial region

$$q_n \vec{u}_n \cdot \nabla \psi_n = \vec{u}_n \cdot \nabla B_n. \tag{7}$$

Above this region, $\vec{u}_n \cdot \nabla \psi_n = 0$ by definition. Also, the streamfunction and potential vorticity are related by $\nabla q_n \times \nabla \psi_n = 0$, and from this and (7)

$$\vec{u}_n \cdot \nabla q_n = o \quad \& \quad \vec{u}_n \cdot \nabla B_n = 0. \tag{8}$$

So, in this equatorial region both q_n and B_n are conserved on streamlines and hence they may be related to one and another on each layer by the function Q_n such that

$$q_n = Q_n(B_n) \tag{9}$$

i.e. when B_n is constant on a streamline (q_n must be also). Assuming the flow is once again hydrostatic the pressure p on layers 1 and 2 may be represented in terms of the depth h such that $p_2 = h, p_1 = h + \Gamma_{12} h_1$ for $\Gamma_{i,j} = \frac{\gamma_i}{\gamma_j}$. Writing the relationship between potential vorticity and B for layer 2 in full,

$$\frac{y - \frac{\partial u_2}{\partial y}}{h_2} \quad = \quad Q_n(h + \frac{1}{2}u_2^2). \tag{10}$$

For geostrophic balance of u_2, we must have $\frac{\partial h}{\partial y} = -y u_2$. We have defined systems of equations that describe both the large f midlatitude regions and those of small f close to the equator. It is now pertinent to merge the two solutions and derive a solution for the full system.

2 Linking the equatorial and mid-latitude regions

The physically important question now arises as to what Q_2 must be in order to link the equatorial regions to those of the multitudes in a consistent way. For large y (where y is a coordinate of the equatorial region), the solutions must merge. About the transition region on layer 2

$$q_2 \approx \frac{y}{h_2} \qquad B_2 \approx h. \tag{11}$$

Using (11) from the ventilated thermocline solution we have

$$Q_2(B_2) \quad = \quad \frac{y_2}{B_2} \tag{12}$$

and hence

$$\frac{y - \frac{\partial u_2}{\partial y}}{h_2} \quad = \quad \frac{y_2}{h + \frac{1}{2}u_2^2}. \tag{13}$$

As Joe pointed out in the principal lectures, equation (13) is the water parcel analogy to marriage. A girl with a lot of potential (y_2) is united with a boy of great thickness (h_2) at high latitudes. Together the flow of life takes them to lower latitudes and although the girl develops added spin ($\frac{\partial u_2}{\partial y}$) and the boy becomes more energetic ($\frac{1}{2}u_2^2$), the relationship between the now man and woman remains the same. However, as Antonello points out, there is a lot of turbulence in the world and such simple models are often not able to be generalized. It is left to the reader to derive

a relationship incorporating turbulent terms (both theoretically and experimentally).We may now simply define the following set of ODEs in y only.

$$\frac{\partial u_2}{\partial y} = y - \frac{y_2}{h + \frac{1}{2}u_2^2}; \tag{14}$$

$$\frac{\partial h}{\partial y} = -yu_2; \tag{15}$$

$$h_2 = h - h_1. \tag{16}$$

In order for the system defined above to be solved we require a relationship between the depth h and thickness of layer 2 h_2. As the solution must hold for the equatorial regions, the Sverdrup relation breaks down and may not be applied here. We will thus attempt to match the solutions at the equatorial boundary. It is feasible to add additional layers, because it is simply the relationship between h_1 and h_2 that we desire. Indeed the inclusion of additional layers reduces the influence of our assumptions about h at the surface.

We will apply two closure techniques. In both cases we allow the solutions to merge at $y_n >> 1$. The first closure assumes that

$$h(x, y) = h(x, y_n) \tag{17}$$

for all y and the second assumes

$$h(x, y) = h_1(x, y_n) + \frac{h(x, y_n) - h(x, y)}{\Gamma_{12}}, \tag{18}$$

which implies that the upper layer *pressure gradient* is independent of y (a somewhat 'sketchy' assumption that should suffice for the present). In order to conserve potential vorticity we may allow no normal flow across the equator. So at $y = 0$ $B_2 = const. = B_0$ where $B_o = h(0, y_n)$. So B_0 will be the final value of h as it makes a transition from higher latitudes to y=0 (figure 1). Thus

$$u_2 h_2 = \frac{1}{q_2}\frac{\partial B_2}{\partial y} = -\frac{\partial}{\partial y}\left(\frac{B_2^2}{2y_2}\right). \tag{19}$$

Thus integrating from $y = 0$ to y_n

$$\int_0^{y_n} u_2 h_2 dy = \left[-\left(\frac{B_2^2}{2y_2}\right)\right]_0^{y_n} = \frac{B_0^2 - h^2(0, y_n)}{2y_2}. \tag{20}$$

This integration may now be carried out for each x so that the closure is met at large y and $B_2 = B_0$ at $y = 0$ for all x. This is done by the 'shooting' method, where u_2 is guessed at $y = y_n$ in an attempt to 'hit' B_0, with the u_2 guess being adjusted at each attempt. The method is repeated iteratively until convergence to a solution for u and h. Figure 2 shows solutions, using the second closure, gained through this method for various points in the domain. An interesting result is the prediction of increased zonal velocity close to the equator. The feature is known as the Equatorial Undercurrent (EUC). Indeed the increase in deep flow is coincident with shallowing of the thermocline from west to east (Figure 3). The same essential result is gained using the alternative closure (Figure 4).

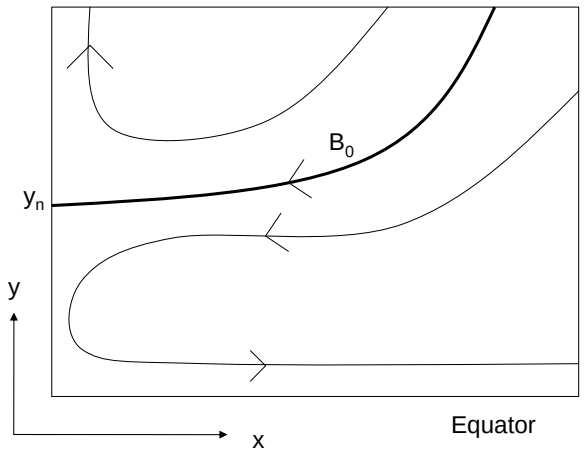

Figure 1: Image showing how B_o is defined at y_n as $h(0, y_n)$ defining a boundary higher and lower latitudes.

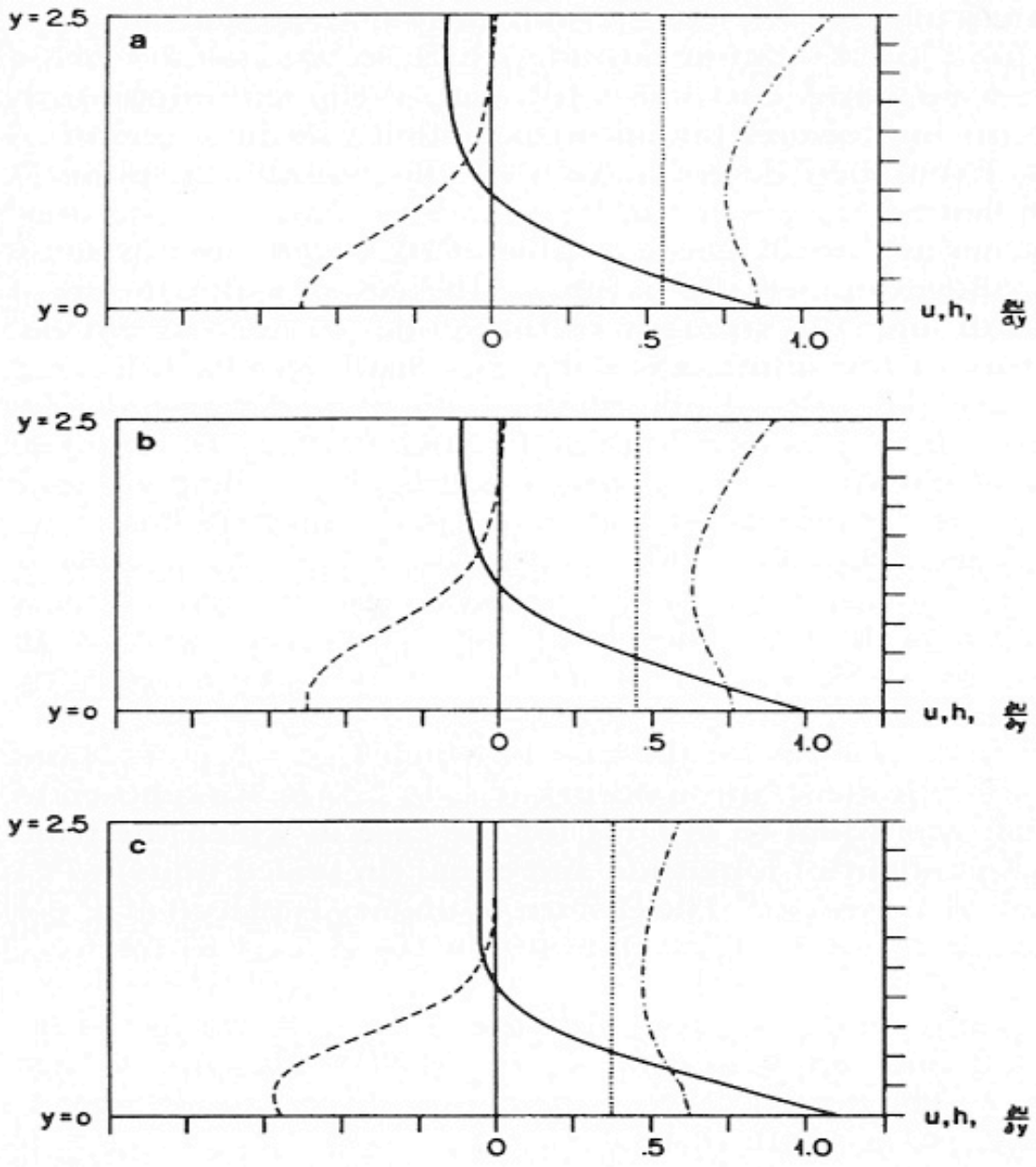

Figure 2: Solutions of (20) for u_2 (solid line), $\frac{\partial u_2}{\partial y}$ (dashed line) and h (dashed-dotted). In this case $\Gamma_{12} = 1$ (second closure). The three panels correspond to profiles at x=0.25, 0.50 and 0.75 respectively. $B_0 = 1.265$ and $y_2 = 5$. Pedlosky (1987)

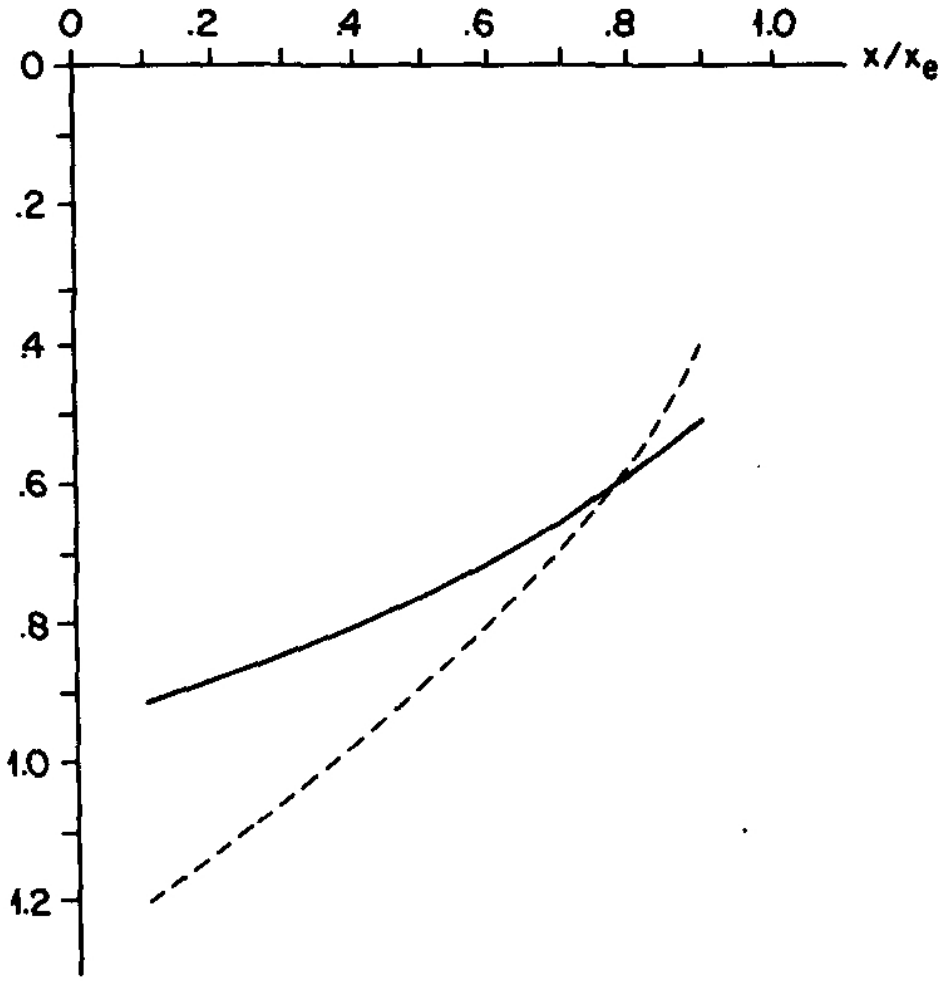

Figure 3: Depth of the base of the moving thermocline layer representing the core of the undercurrent shown as a *solid line* at the equator and as a *dashed line* in the matching region at $y = y_n$. Pedlosky (1987)

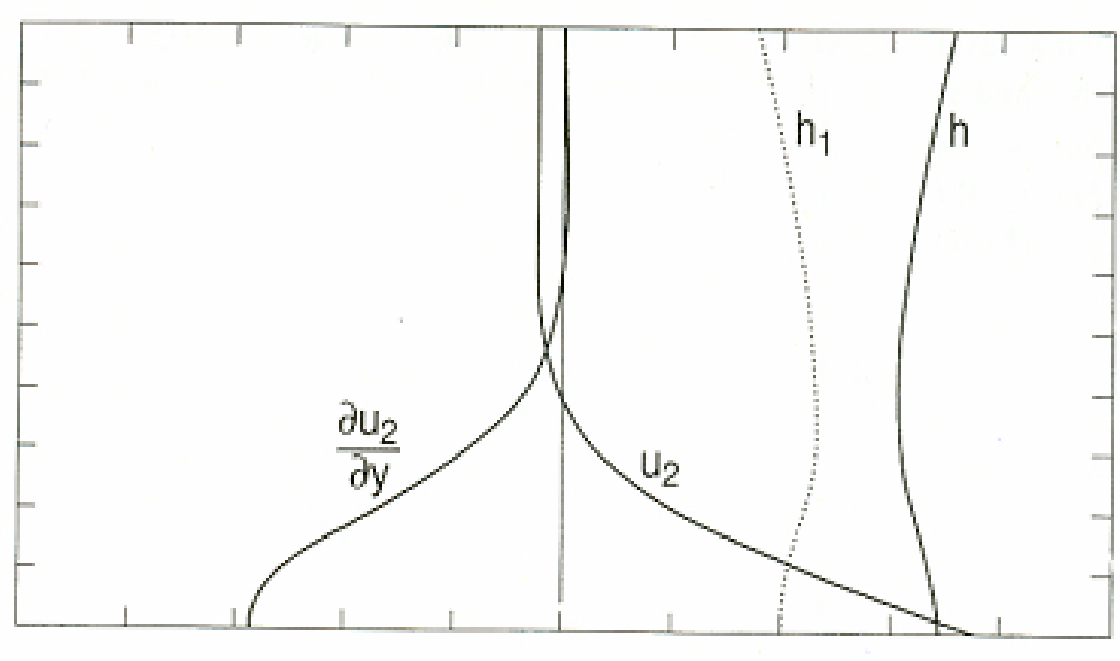

Figure 4: Profiles of u_2, $\frac{\partial u_2}{\partial y}$, h, and h_1 for the case in which (17) is satisfied. The parameters are otherwise as in Figure (2). The calculation is at $x = 0.5$. The maximum eastward velocity is now 0.910.

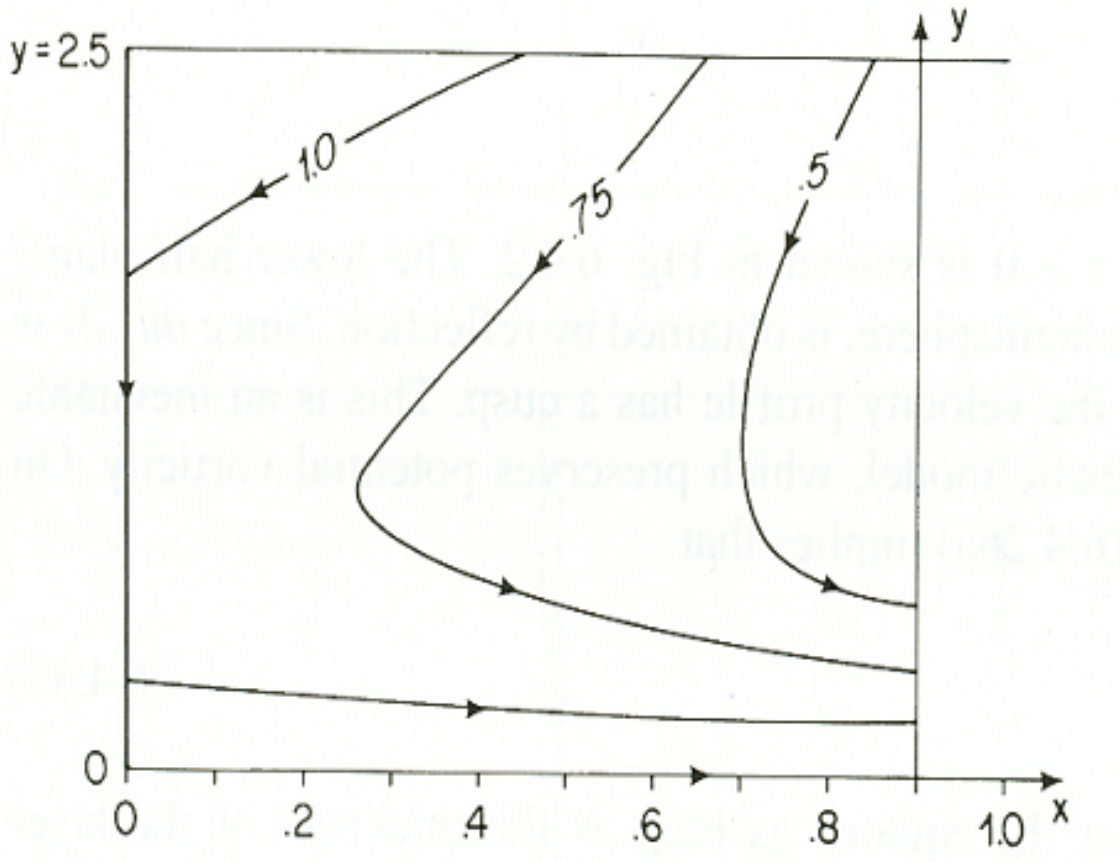

Figure 5: Lines of Constant B_2, which are surrogates for streamlines, calculated from results of 2nd matching (figure 2). Pedlosky (1987)

Analyzing the Bernoulli function B_2 on layer 2 reveals the structure of the undercurrent (Figure 4) as lines of constant B are surrogates of streamlines. The flow is largely southward from the matching region and steers towards the East as the equator is approached.

Modifications to this model, allowing for multiple layers, have been made and show that the undercurrent is still present on deeper layers and reduces in magnitude away from the surface (Figure 6). Indeed, this undercurrent is observed and known as the equatorial undercurrent (EUC)

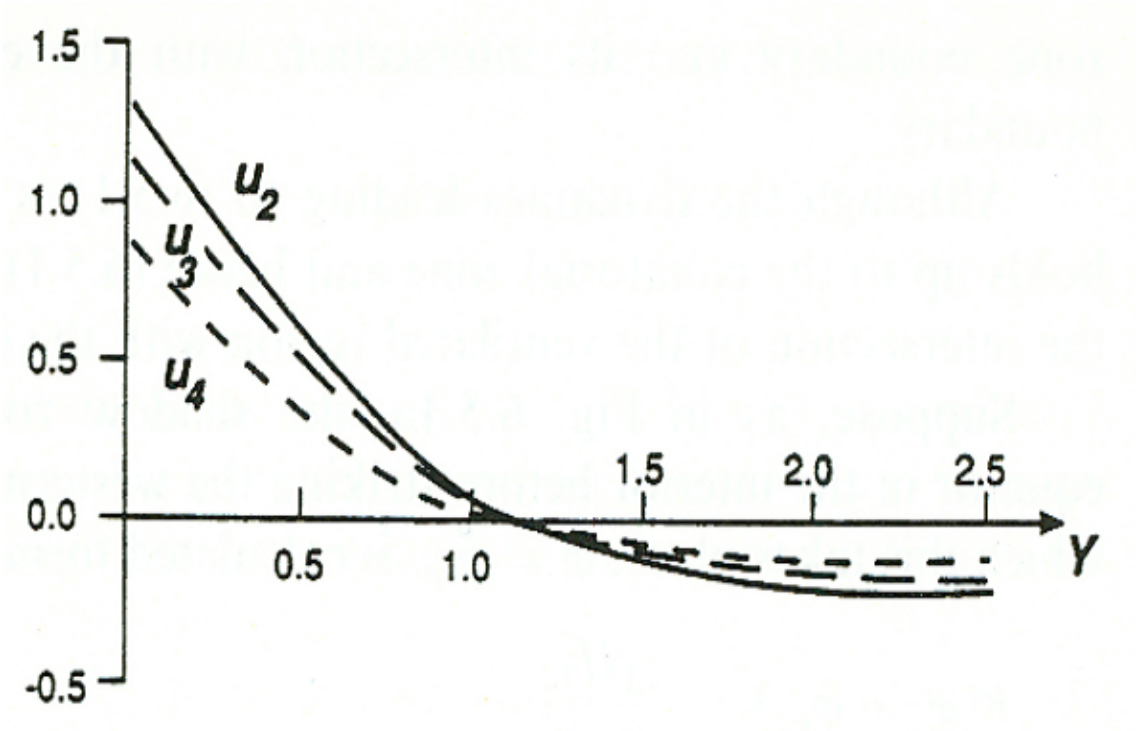

Figure 6: Results of a four-layer model showing the monotonic decrease of the velocity with depth in the undercurrent solution. (Courtesy of R Samelson, pers. comm.)

and has been observed as a clear zonal velocity maximum at around 120m depth in the Atlantic and observed also in the Pacific (Figures 7 and 8). Numerical studies also predict this inertially driven EUC (Figure 9).

3 The Internal Boundary Layer in the Thermocline

We now turn our attention to the boundary between the warm surface waters of the thermocline and the dense abyssal waters derived from the poleward regions. We wish to consider the interaction between the coldest water in the subtropical thermocline downwelled from the equatorward boundary of a subpolar gyre and the denser waters below. In order to have a smooth transition between these two regions, it has been anticipated Welander (1971) that a diffusive 'internal' layer might exist. In order to explore this layer and its effect on the ocean and its sensitivity to the magnitude of vertical diffusivity, we follow the approach of Samelson and Vallis Samelson and Vallis (1990).

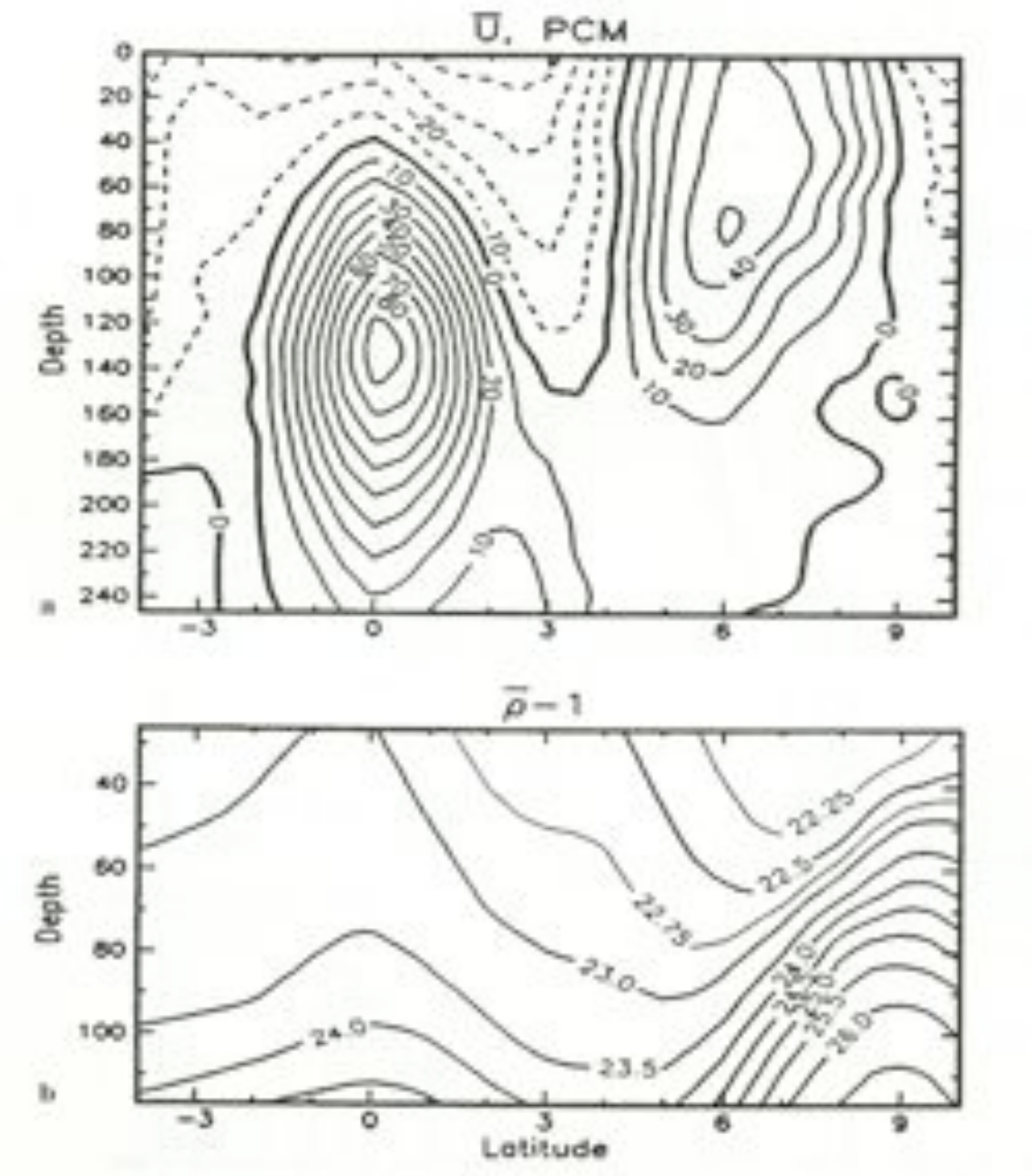

Figure 7: Panel **a** shows contours of zonal velocity measured using current meters in the Pacific. Panel **b** show the density field of the same region. It should be noted that the meridional density gradient vanishes at the equator. Johnson and Luther (1994)

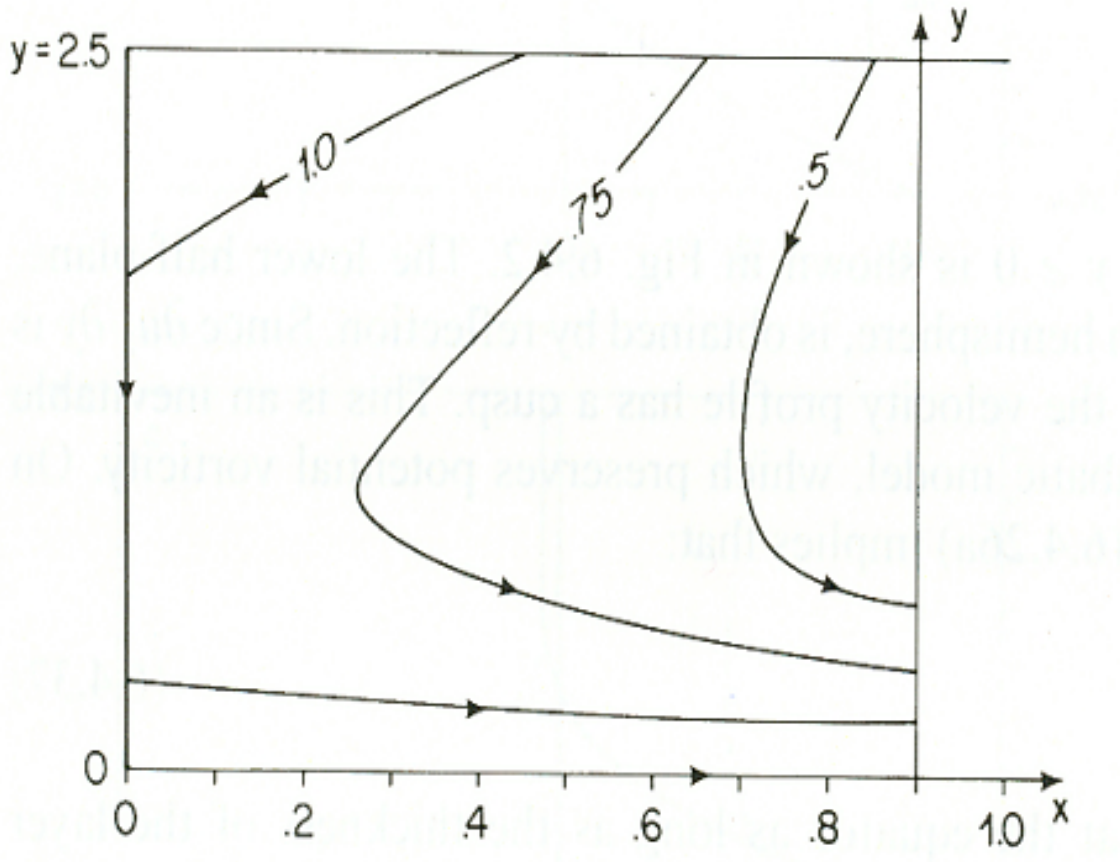

Figure 8: Evidence of the EUC from temperature and zonal velocity profiles from the Atlantic and Pacific Oceans. In each case measurements represent 2-year means. Halpern and Weisberg (1994)

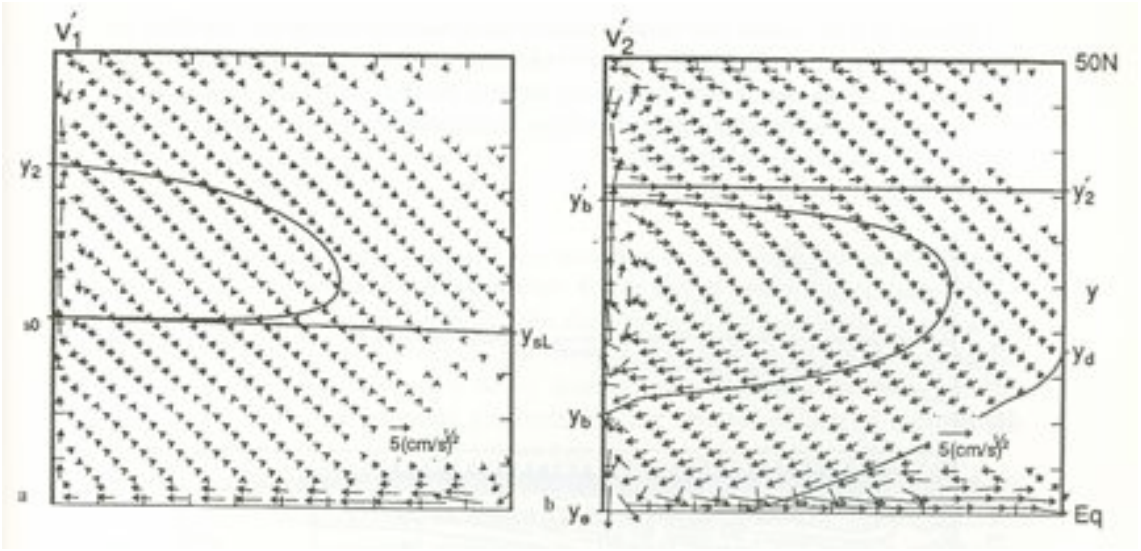

Figure 9: Numerical studies McCreary (1994) show a shadow zone which strikes the equator within the basin. In this case the EUC is fed from the subtropical gyre through the interior as well as the western boundary current.

By assuming a geostrophic and Boussinesq fluid we may define the following set of equations:

$$-fv = -\frac{\partial p}{\partial x} - \epsilon u \quad , \quad -fu = -\frac{\partial p}{\partial y} - \epsilon v, \tag{21}$$

$$\frac{\partial u}{\partial x} + \frac{\partial v}{\partial y} + \frac{\partial w}{\partial dz} = 0. \tag{22}$$

Here a traditional (and somewhat unsatisfying) friction term ϵ is included to avoid singularities in $\mathbf{u}$ when f=0. We shall assume that the fluid is hydrostatic and conserve buoyancy ($b = \frac{\rho - \rho_0}{\rho} g$) such that

$$b_t + ub_x + vb_y + wb_z = \kappa_v b_z z + \kappa_H \nabla^2 b - \lambda \nabla^4 b \quad \& \quad \frac{\partial p}{\partial z} = b, \tag{23}$$

and the Laplacian is defined only in the horizontal ($\nabla^2 = \frac{\partial^2}{\partial x^2} + \frac{\partial^2}{\partial y^2}$). Specifying the Ekman pumping and applying typical boundary conditions, a double structure of the thermocline is revealed (Figure 10). The temperature gradient in (10) reveals a local maxima at which point the vertical velocity switches from a downward pumping to a deep *positive* w, which reduces with depth. Since w is zero at the base of the adiabatic thermocline and the horizontal gradient of buoyancy is determined by the slope of the isopycnals in the ventilated thermocline solution we may use the scalings

$$\frac{\partial w}{\partial z} = \frac{\beta}{f} v \quad \Rightarrow \quad W = \frac{\beta}{f} U \delta \tag{24}$$

$$u_z = -b_y / f \quad \Rightarrow \quad \frac{\Delta b}{L} = \frac{fU}{D_a}, \tag{25}$$

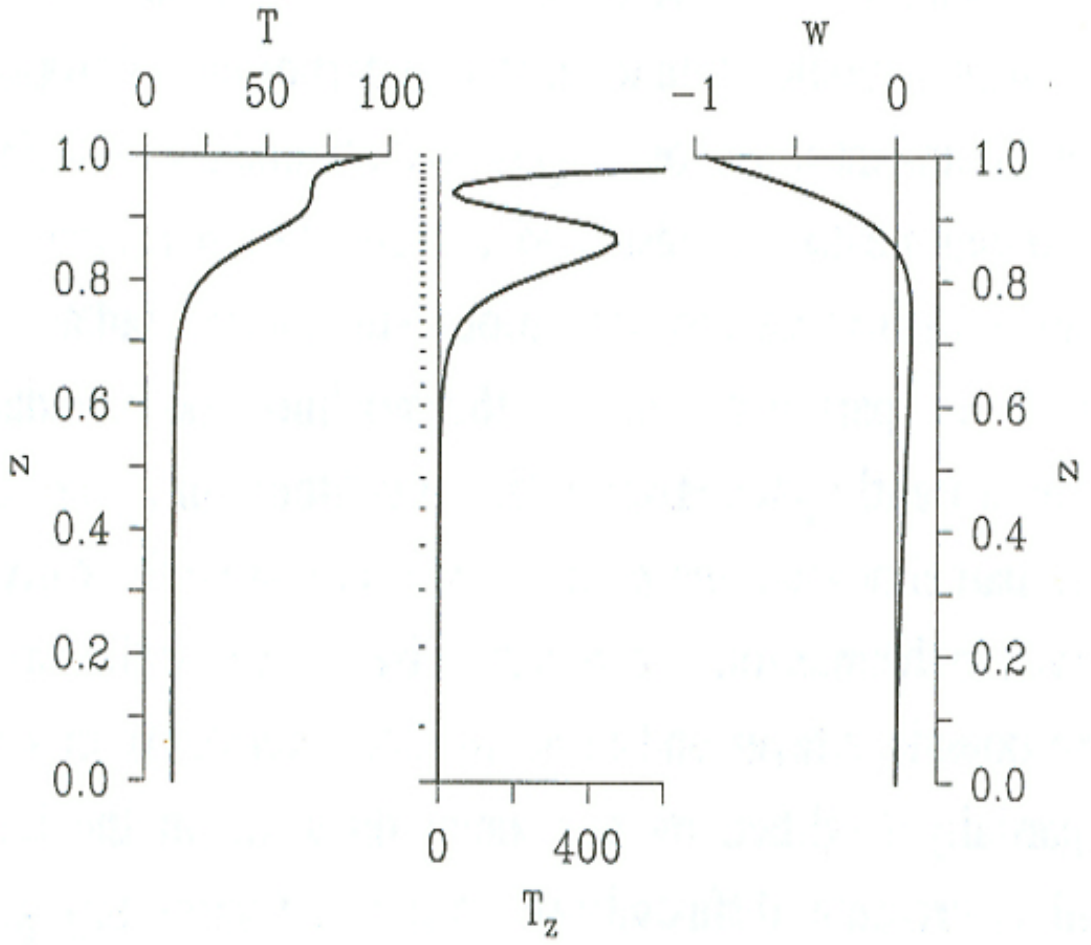

Figure 10: Vertical profiles of T (left panel), T_z (centre), and w (right) at the centre of the domain, (x,y)=(0.5,0.5)

and hence we define the vertical scale of the adiabatic thermocline D_a as

$$D_a^2 \frac{f^2 W_e L}{\beta \Delta b}. \tag{26}$$

We see that in the region of the internal thermocline, vertical diffusion balances vertical advection (Figure 11) such that $wT_z \approx \kappa T_{zz}$ (in this model T is a proxy for b) and such that the vertical velocity scales by W/δ $\kappa_v \delta^2$. Again using scalings (24) and (25) we have

$$W_e = \frac{\beta}{f}\frac{\Delta b}{L} D_a \delta = \frac{\kappa_v}{\delta} \quad \& \quad \delta = \left(\frac{\kappa f L}{\beta \Delta b D_a}\right) \tag{27}$$

$$\Rightarrow \delta = \kappa_v^{1/2} \left(\frac{\kappa f^2 L}{\beta \Delta b W_e}\right)^{1/4} \tag{28}$$

Here we have uncovered a $\kappa_v^{1/2}$ relationship by using the scaling height δ which is the scale over which the velocities u and w vary rather than the scale of the thermocline D_a which yields a $1/3$ power law. Analysis of the model of Samelson and Vallis indeed reveals the $1/2$ power law as shown in figure (12). So Samelson and Vallis, with their simple thermocline model, establish that the flux through the internal boundary is intrinsically diffusive, scaling as $\kappa_z^{1/2}$. Indeed others have treated the internal boundary layer problem in a different way, looking at the entirety of the Thermocline as a diffusive boundary layer. Salmon (1990) looks at this problem and combines the geostrophic balance relationships

$$fv = \frac{1}{\rho_0}\frac{\partial P}{\partial x} \quad \& \quad \beta v = f \frac{\partial w}{\partial z} \tag{29}$$

to get

$$\frac{1}{\rho_0}\frac{\partial P}{\partial x} \quad = \quad \frac{f^2}{\beta}\frac{\partial w}{\partial z}. \tag{30}$$

It is implied from the above that there exists some function M such that

$$\frac{1}{\rho_0} P = M_z \quad \& \quad \frac{f^2 w}{\beta} = M_x \tag{31}$$

and therefore

$$u = -\frac{M_{zy}}{f}, \quad v = \tfrac{M_{zx}}{f}, \quad \frac{g\rho}{\rho_0} = M_z z. \tag{32}$$

From density conservation ($\mathbf{u} \cdot \nabla \rho = \kappa_v \rho_z z$) the following relationship for M results

$$\frac{1}{f}\left[M_{zx} M_{zzy} - M_{zy} M_{zzx}\right] + \frac{\beta}{f^2} M_x M_{zzz} = \kappa_v M_z zzz. \tag{33}$$

If we take the simple case where $M = M(x, z)$, using the scaling factors L, U, d, g' and W and writing (29) and the one dimensional density equation ($w\rho_z = \kappa_v \rho_z z$) in terms of these gives

$$\frac{U}{d} = \frac{g'}{fL}, \quad U = \tfrac{fW}{\beta d}, \quad W = \frac{\kappa_v}{d} \tag{34}$$

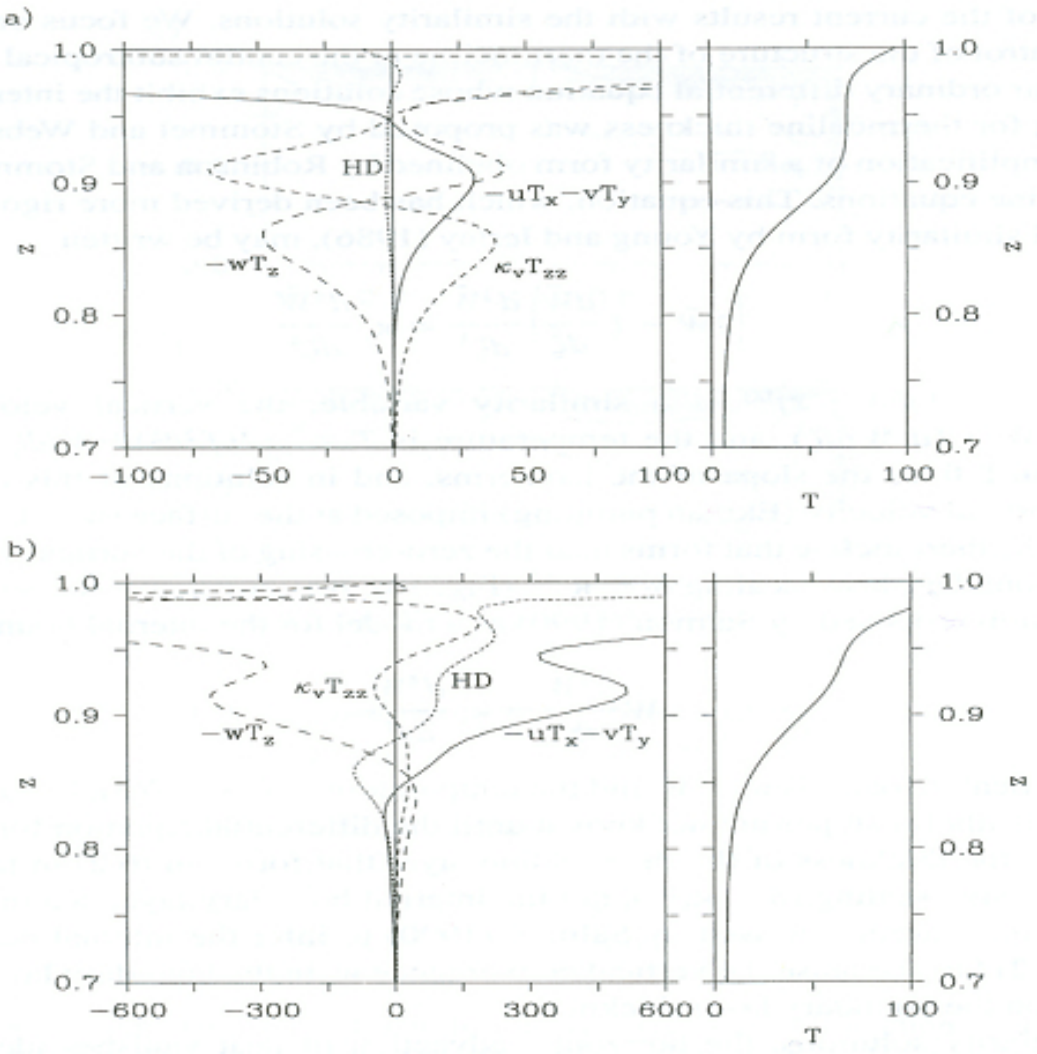

Figure 11: Vertical profiles of terms in the thermodynamic equation for $K_h = 0.002$ with $K_v = 0.003$ at (a) the centre of the domain, (x,y)=(0.5,0.5), and (b) near the western boundary, (x,y)=(0.024,0.5). The profiles for horizontal advection $(-uT_x - vT_y)$, vertical advection $(-wT_z)$, vertical diffusion $(\kappa_v T_z z)$ and the horizontal (Laplacian plus biharmonic) diffusion (HD) are labeled accordingly. The corresponding profiles of T are also shown (right panels). The units are $T_*/t_* = 5.4 \times 10^{-4}\mathrm{Kyr}^{-1}$.

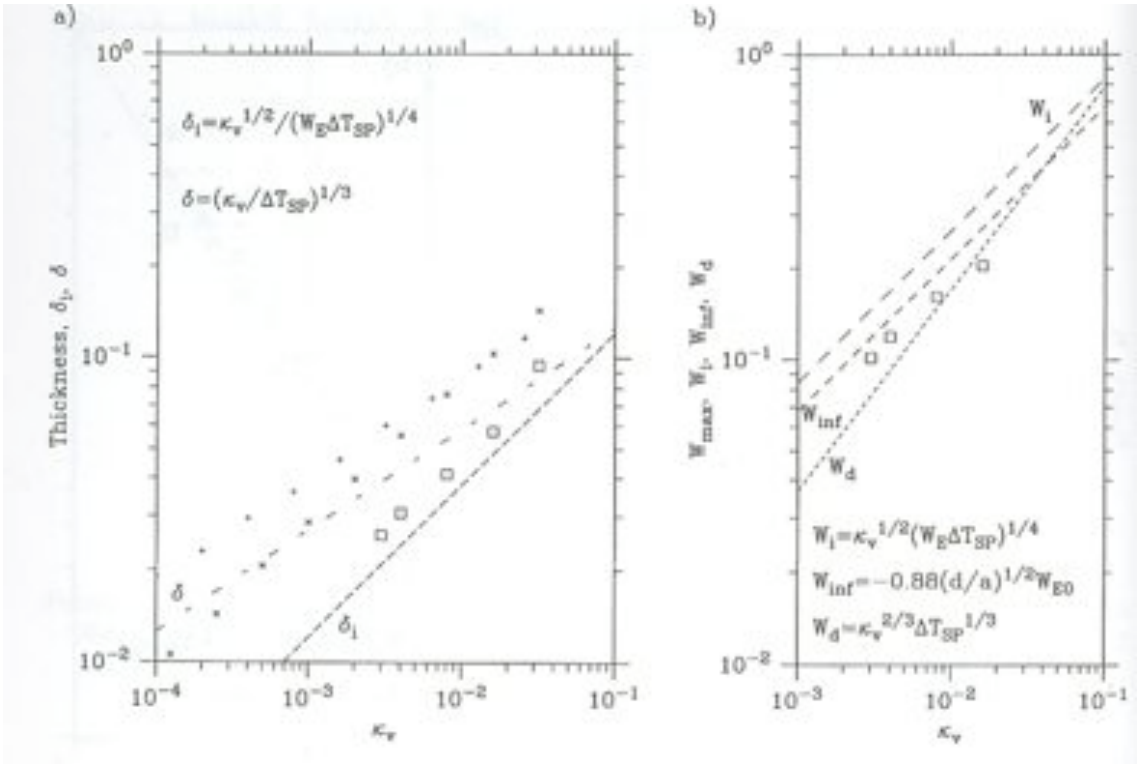

Figure 12: (a) Thickness of the internal peak of T_z versus κ_v, from the profiles in Figure 11. The internal boundary layer scale δ_i and the advective-diffusive scale δ are also shown (dashed lines), along with the corresponding thickness from solutions of the similarity equations (...) and (...). (b) Maximum upward vertical velocity at (x,y)=(0.5,0.5) versus κ_v, from solutions in Figure 11. The internal boundary layer scale W_i, the asymptotic estimate $W_{inf} = W_{\rm inf}$ and the advective-diffusive scale W_d are also shown (dashed lines).

and hence

$$d = \left(\frac{\kappa_v f^2 L}{\beta g'}\right)^{1/3} \quad \& \quad W = \kappa_v^{2/3}\left(\frac{\beta g'}{f^2 L}\right). \tag{35}$$

So, by this simple scaling argument we have found evidence for a thicker boundary layer and a weaker vertical flow w below the thermocline. Solutions of the one-dimensional version of equation (33) with appropriate boundary conditions applied at the surface and ocean bottom are shown in figure (13). These indeed show a deeper boundary layer and small vertical velocity in the interior.

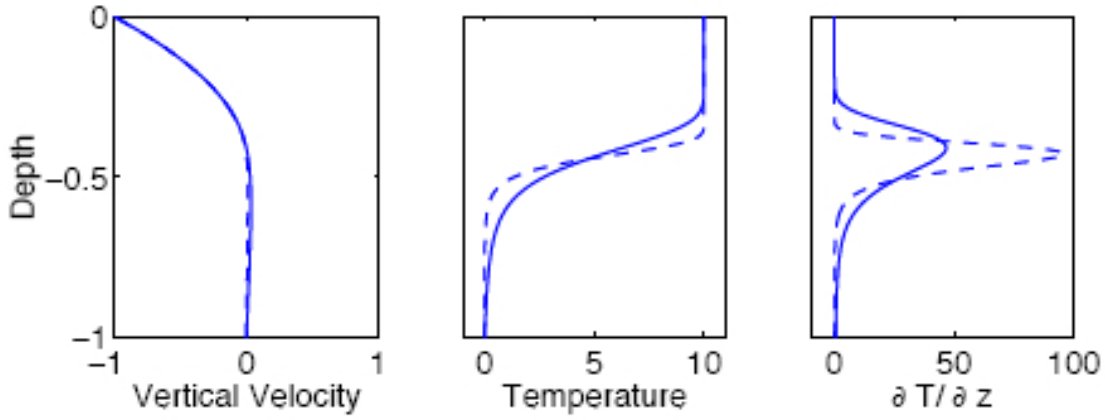

Figure 13: Solution of the one dimensional version of thermocline equation (33) for two different values of the diffusivity: $\hat{\kappa} = 3.2 \times 10^{-3}$ (solid line) and $\hat{\kappa} = 0.4 \times 10^{-3}$ (dashed line), in the domain $0 \le \hat{z} \le -1$.'Vertical velocity' is W, 'temperature' is $-W_{\hat{z}\hat{z}}$, and all units are the non-dimensional ones of the equation itself. A negative vertical velocity, $\hat{W}_E = -1$, is imposed at the surface (representing Ekman pumping) B_0=10. The inertial boundary layer thickness increases as $\hat{\kappa}^{1/3}$, so doubling in thickness requires an eightfold increase in $\hat{\kappa}$. The upwelling velocity above the internal boundary layer is much larger and almost independent of $\hat{\kappa}$. The depth of the boundary layer increases as $\hat{W}_E^{1/2}$, so if $\hat{W}_E = 0$ the boundary layer is at the surface. Vallis (2006)

Somewhat different one-dimensional thermocline models have been described, and these have slightly different scaling properties. However, their qualitative features are very similar. For example, in both cases the thickness of the internal thermocline increases with increasing diffusivity (κ_v), and the thickness gets smaller with increasing temperature difference across it. The strength of the vertical velocity increases with increasing diffusivity also. This has an obvious implication for the overturning circulation as the upwelling velocity is an integral component of it.

References

D. Halpern and R. H. Weisberg. Upper Ocean thermal and flow fields at 0^o, 28^oW (Atlantic) and 0^o, 140^oW (Pacific). 10:7651–7664, 1994.

E. S. Johnson and D. S. Luther. Mean zonal momentum balance in the upper and central equatorial Pacific Ocean. 10:7651–7664, 1994.

J.P. Jr. Lu P. McCreary. The interaction between the subtropical and equatorial circulations: The subtropical cell. 24:466–497, 1994.

J. Pedlosky. An Inertial Theory of the Equatorial Undercurrent. 17:1978–1985, 1987.

R.M. Samelson and G.K. Vallis. Large-scale circulation with small diapycnal diffusion: the two thermocline limit. 55:223–275, 1990.

G. K. Vallis. *Atmospheric and Oceanic Fluid Dynamics: Fundamentals and Large-Scale Circulation*. Cambridge University Press, Cambridge, U.K., 2006.

P. Welander. The Thermocline Problem. *Phil. Trans. R. Soc. Lond. A*, 270:415–421, 1971.